European Heart Journal (2010) **31**, 1410–1420
doi:10.1093/eurheartj/ehp547

In vivo labelling of resting monocytes in the reticuloendothelial system with fluorescent iron oxide nanoparticles prior to injury reveals that they are mobilized to infarcted myocardium

Karin Montet-Abou[1†], Jean-Luc Daire[1†], Jean-Noël Hyacinthe[1], Manuel Jorge-Costa[2], Kerstin Grosdemange[3], François Mach[4], Alke Petri-Fink[5], Heinrich Hofmann[5], Denis R. Morel[2], Jean-Paul Vallée[1], and Xavier Montet[1,3*]

[1]Radiology Department, Geneva University Hospital, Geneva, Switzerland; [2]Anesthesiological Investigation Unit, Anesthesiology, Pharmacology and Intensive Care Department, Geneva University, Geneva, Switzerland; [3]Cell Physiology and Metabolism Department, Geneva University, Michel-Servet 1, 1211 Geneva 14, Switzerland; [4]Cardiology Department, Geneva University Hospital, Geneva, Switzerland; and [5]Laboratory of Powder Technology, Ecole Polytechnique Fédérale de Lausanne (EPFL), Lausanne, Switzerland

Received 8 January 2009; revised 24 September 2009; accepted 17 November 2009; online publish-ahead-of-print 19 December 2009

Aims To evaluate the feasibility of loading resting monocytes/macrophages by intravenous (i.v.) injection of fluorescent iron oxide nanoparticles prior to injury and tracking of these cells in the very same animal to myocardial infarction (MI) by magnetic resonance imaging (MRI) and optical imaging.

Methods and results Rats were injected with fluorescent iron oxide nanoparticles (10 mg/kg) ($n = 15$) prior to injury. After disappearance of the nanoparticles from the blood, MI was induced. Monocytes/macrophages were then tracked in the very same animal by MRI and optical imaging. Control groups were (i) non-injected animals ($n = 15$), (ii) injected animals associated with a sham operation ($n = 8$), and (iii) animals treated with an anti-inflammatory agent ($n = 6$). The presence of iron-loaded cells can be detected by MRI *in vivo* in the infarcted myocardium. Here, we showed that the detection of inflammatory cells *in vivo* correlated well with *ex vivo* imaging (MRI and reflectance fluorescence) and histology. We also showed that the method is robust enough to depict changes in the inflammatory response.

Conclusion This study demonstrates that resting monocytes/macrophages can be loaded *in vivo* by a simple i.v. injection of fluorescent superparamagnetic iron oxide nanoparticles prior to injury and then tracked, in the same animal, in a model of ischaemia–reperfusion leading to myocardial infarct. Although previous studies of macrophages infiltration following MI have labelled the macrophages after injury, this study, for the first time, has pre-load the resting monocytes with fluorescent iron oxide nanoparticles.

Keywords Magnetic resonance imaging • Iron oxide nanoparticles • Inflammation • Myocardial infarction

Introduction

The inflammatory response following myocardial infarction (MI) is well documented.[1–3] Pro-inflammatory cytokines, like TNF-α, IL-1β, and IL-6 are found in MI within the first hours to the first days. Monocyte chemoattractant protein-1 (MCP-1) is also up-regulated in MI.[4,5] Altogether, these cytokines attract inflammatory cells into the MI zone, including mast cells and monocytes/macrophages. Once these cells have transmigrated into the MI, they will also produce cytokines and the heart enters into a vicious cycle of cytokine amplification that could be either favourable, leading to healing, or deleterious, leading to heart remodelling and ultimately to heart failure. Hence, *in vivo* visualization of inflammatory cells after MI would be of primary

† These authors contributed equally to this work.

* Corresponding author. Tel: +41 22 379 57 84, Fax: +41 22 379 52 60, Email: xavier.montet@hcuge.ch

importance to better define at which time the inflammatory response is favourable or deleterious.

Distinguishing cells of interest from complex background implies that cells have to be tagged with a contrast medium that could be observed through imaging modalities. Many reports used *ex vivo* cell loading with transfection agents and have already proven that cell tracking can be realized *in vivo*.[6] Nevertheless, the use of transfection agents is not straightforward[7] and *ex vivo* manipulation of cells can activate and/or modify their biological behaviour.[8] From this point of view, it would be interesting to load the cells *in vivo* and to track them *in vivo* in the same animal. It is well known that nanoparticles are cleared from the blood by the reticuloendothelial system (RES).[9] Hence, the monocytes/macrophages system could be loaded *in vivo* by a simple intravenous (i.v.) injection of nanoparticles.

Iron oxide nanoparticles are potent contrast agents for magnetic resonance imaging (MRI) and are FDA approved for clinical use. Magnetic resonance imaging is a modality of choice for *in vivo* imaging because the technique is (i) non-invasive, allowing serial imaging of the very same animal, (ii) non-ionizing, and (iii) sensitive enough to detect iron-loaded cells in a living animal,[9] as well as in human.[10]

The goal of this paper was to load resting monocytes/macrophages *in vivo* with fluorescent iron oxide nanoparticles before inducing an inflammatory lesion in rats. Once the nanoparticles have been cleared from the plasma, an ischaemia–reperfusion episode of the heart was realized to induce an acute and localized inflammation. The monocytes/macrophages infiltration of the MI was then tracked *in vivo* by MRI in the very same animal and cell infiltration confirmed by *ex vivo* MRI, reflectance fluorescence, and histology.

Methods

Fluorescent iron oxide nanoparticles

To synthesize fluorescent iron oxide nanoparticles, superparamagnetic iron oxide nanoparticles (SPION) containing amino groups on their surface, synthesized as described previously,[11,12] were reacted with *N*-hydroxysuccinimide ester of FluoProbes 565 (absorption = 563 nm/emission = 592 nm) (Fluoprobes, Interchim, France). There were ~1000 amino groups on each nanoparticle with four to five amines consumed for the attachment of the fluorophores.

Plasma half-life and whole blood fluorescence

All animal experiments were approved by the Ethics Committee of our university and were in accordance with the Swiss guidelines for animal experiments.

To determine whole blood fluorescence and plasma half-life of the nanoparticles, 10 mg/kg of fluorescent SPION were injected into the tail vein of Sprague–Dawley rats weighing 322 ± 12 g ($n = 2$). Two hundred microlitres of blood were collected in heparinized tubes before, immediately after i.v. injection, and at 2, 4, 8, 24, and 48 h post-injection. Whole blood and plasma (obtained after 12 min centrifugation at 500 *g*) optical density was read at 563 nm on a DU 730 spectrophotometer (Beckman–Coulter, Fullerton, CA, USA). To determine in which cells the fluorescence reappeared in whole blood, leucocytes were purified on Ficoll gradient (Ficoll-Paque PLUS, GE Healthcare, Uppsala, Sweden) and then analysed by immunohistochemistry against CD68 (and against PMN, data not shown) (see below).

Animal model of ischaemia–reperfusion

All surgeries, i.v. injection, and MRI were realized under 2–3% isoflurane inhalation anaesthesia (Isoflurane, Baxter, IL, USA).

Under isoflurane anaesthesia, tracheal intubation, and mechanical ventilation, the left femoral artery was cannulated to allow continuous monitoring of arterial pressure. A three-lead electrocardiogram (ECG) using subcutaneous electrodes was placed, allowing monitoring the ischaemia in real time. A balanced electrolyte solution (0.5 mL/100 g/h) was infused to compensate for insensible fluid losses. After an i.v. bolus of fentanyl (10 μg/kg) for supplemental analgesia, the heart was exposed through a left thoracotomy. A 6-0 polypropylene suture was placed around the left anterior descending (LAD) coronary artery close to its origin and maintained occluded for 30 min. The occlusion of the LAD coronary artery was confirmed by ECG changes (ST-segment elevation), regional cyanosis, and akinesia of the anterior ventricular area. After 30 min of ischaemia, the polypropylene suture was completely removed, allowing reperfusion.

After haemodynamic stabilization (30 min), the chest was closed. To alleviate post-operative pain, the wounds were infiltrated with a local anaesthetic (bupivacaine 0.125%, 1 mL) and buprenorphine (0.05 mg/kg every 12 h for 48 h) was injected subcutaneously. After full anaesthesia emergence, the rats were closely monitored and allowed free access to standard rat chow and water.

Animal groups

Animals were divided into four groups. The first one ($n = 15$, weighing 310 ± 8 g) received an i.v. injection of fluorescent SPION (10 mg/kg) 3 days before the ischaemia–reperfusion. Magnetic resonance imaging was performed on this group every day from Days 0 to 3. Each day, three animals were sacrificed for subsequent *ex vivo* imaging and histological correlation. This group was denoted SPION_MI. The second group ($n = 15$, weighing 329 ± 13 g) was not injected with fluorescent SPION but underwent the same ischaemia–reperfusion protocol as the SPION_MI group and was also imaged from Days 0 to 3. Each day, three animals were sacrificed for subsequent *ex vivo* imaging and histological correlation. This group was denoted Ø_MI. The third group ($n = 8$, weighing 317 ± 15 g) received an i.v. injection of fluorescent SPION (10 mg/kg) 3 days before surgery. For this group, the 6-0 polypropylene suture was placed around the LAD but not closed (=Sham group), denoted SPION_Sham. Magnetic resonance imaging was acquired from Days 0 to 3. Animals were sacrificed at Day 0 ($n = 2$) and Day 3 ($n = 6$). The fourth group ($n = 6$, weighing 311 ± 16 g) was injected with fluorescent SPION (10 mg/kg) 3 days before surgery. This group underwent the same ischaemia–reperfusion as the SPION_MI and Ø_MI groups but received an anti-inflammatory treatment immediately after the beginning of the reperfusion. The anti-inflammatory treatment consisted of an intraperitoneal (i.p.) injection of 333 μg/kg of [^{44}AANA^{47}]-RANTES, a potent anti-CCL5 agent.[13] This group was denoted SPION_MI_AntiCCL5. All animals were sacrificed after the last imaging session by i.v. injection of KCl (200 mEq/kg). The heart was then imaged *ex vivo* by fluorescence imaging and by MRI. At the end of the *ex vivo* imaging session, the heart was quick-frozen and stored at −80°C for subsequent histological analysis.

Magnetic resonance imaging

All images were acquired on a clinical scanner at 1.5 T with a dedicated microscopic surface coil (47 mm diameter) (Philips Medical System,

Best, The Netherlands). Our experimental settings have already been published.[14] Briefly, the rats were placed in a cradle in prone position. A rectal thermal probe with a heating system was used to maintain the temperature of the rats constant (37.0–37.5°C), a respiratory pillow was placed on the abdomen to measure breathing rate. Subdermal electrodes were placed to record an ECG used as a cardiac trigger for the MR system. The monitoring devices were connected with optical fibres to a computer during the MRI acquisitions [SA Instrument, Inc. (SAII), Stony Brook, NY, USA, MR-Compatible Model 1025 Monitoring and Gating System]. Using this set-up, the physiological parameters of the rats were continuously measured in real time during the whole experiment.

Cine imaging was realized using a prospective ECG-triggered segmented turbo field echo cine sequence, TR/TE 12/4.9 ms. Flip angle (FA) 30°, 288 × 288 matrix sampled on a Cartesian grid, 80 mm field of view (FOV), and 2 mm slice thickness yielding an in plane resolution of 280 × 280 μm. Eleven to 20 cardiac phases where acquired per R-R cycle depending on the heart rate. Two short axial planes, as well as two- and four-cavity views, were acquired for each animal.

Tagged MRI was obtained by using a C-SPAMM tag preparation segmented cine fast field echo (FFE) sequence,[15,16] TR/TE 7.8/3.6 ms, tag spacing 1 mm, acquired voxel size 0.31 × 0.31 × 3 mm, and FA 10°. The inter image time was about 8 ms yielding to 18–25 phases per cardiac cycle. Six short axis levels were acquired on each animal.

Fast field echo sequence was used for iron oxide particles detection; TR/TE1/TE2 350/7/15 ms; FA 50°, 395 × 608 matrix sampled on a Cartesian grid, 120 mm FOV, and 2 mm slice thickness with a negative gap of −1 mm yielding an in plane resolution of 200 × 300 μm.

Multi-echo spin echo sequence was used to calculate T2 relaxation time; $TR/TE_{min}/TE_{max}$ 520/5.9/94.4 ms with 16 echoes in-between, 256 × 256 matrix sampled on a Cartesian grid, 80 mm FOV, and 3 mm slice thickness yielding an in plane resolution of 310 × 310 μm. T2 values were calculated according to the equation: signal intensity $= M_0(e^{-TE/T2})$, where M_0 is the initial magnetization, TE is the time of echo.

Total imaging time was <1 h per animal.

Global cardiac function analysis

The left ventricle ejection fraction (LVEF) was assessed for each animal with MR cine images according to: LVEF (%) $= (V_{diast} - V_{syst})/V_{diast}$. End-diastolic ($V_{diast}$) and end-systolic ($V_{syst}$) volumes were calculated by manually drawing endocardial contours and long axis length at end-diastolic and end-systolic phases for each axis. End-diastolic and end-systolic volumes were calculated according to the Simpson's modified method:[17,18] volume $=$ (length/2) $\times$ ($A_{basal} + 2/3 \times A_{apex}$) with A_{basal}, diastolic or systolic basal area; A_{apex}, diastolic or systolic area; length, diastolic or systolic long axis length.

Regional cardiac function by tag analysis

The tag analysis was performed with the Extrema Temporal Chaining algorithm.[19] Extrema Temporal Chaining algorithm consists in tracking points of tag and crest lines along their orthogonal direction by a temporal chaining. These points are detected as local minima and maxima of 1D signals corresponding to lines or columns of the 2D images. In parallel, a spatial smoothness assumption of the deformation field and to the myocardial boundaries is incorporated to prevent abnormal extrema matching. Starting from a spatial chaining on the first image, real 2D displacements are computed on extrema locations. Finally, displacements of all the myocardium points are interpolated via the Laplace equation. Circumferential strains (CS) are then averaged in 12 sectors. Maximum of the CS were measured in the midwall (by dividing the wall thickness in thirds) in per cent according to the formula: $\%CS = (CS_{syst} - CS_{dias})$.

Ex vivo fluorescence imaging

The heart was explanted, rinsed in NaCl 0.9%, and imaged with an IVIS-200 system (Calipers live science AG, Switzerland) using filters of 500–550/575–650 (abs/em). Images were digitally acquired as 16-bit images on a cooled-CCD camera.

Ex vivo magnetic resonance imaging

The heart was placed inside a test tube containing NaCl 0.9% and scanned again with a surface microscopic coil of 23 mm diameter utilizing the same FFE sequence as *in vivo*, but at higher resolution. The in-plane resolution was 100 × 100 μm and the slice thickness 2 mm.

Histological staining

Frozen hearts were cut on a CM3050 cryostat (Leica Microsystems GmbH, Germany). Ten slices of 6 μm every millimetre were collected. Sections were stained with haematoxylin–eosin for morphological analyses; Masson's trichrome for fibrosis quantification and Prussian Blue for iron detection.

Fibrosis was evaluated by hand drawing region of interest. The volume of fibrosis was normalized by the volume of the LV.

Immunohistochemistry was realized on acetone-fixed cryosections, which were blocked with PBS containing 2% BSA, and incubated for 2 h with a mouse anti rat CD68 diluted 1:1000 (Abd Serotec, Oxford, UK). A secondary antibody (goat anti mouse-FITC, Jackson Immunoresearch Europe) was applied at 1:100 for 1 h. Nuclear staining was obtained with a mounting media containing DAPI (Vectashield hard set with DAPI, Vector Laboratories, Burlingame, CA, USA). Control sections were processed identically, with the exception of omitting the incubation with the primary antibody. The controls never showed specific binding.

Monocytes/macrophages numbers per FOV (×400) were counted. Three FOV per level were used to average the number of CD68-positive cells present in the myocardial infarct.

Co-localization of CD68-positive cells with fluorescent SPION was automatically analysed and measured on histological slices with the TissueQuest software (TissueQuest, TissueGnostics, Vienna, Austria). The software allows to automatically detect nuclei of all cells based on nuclear fluorescence. Once all individual nuclei are identified, a measure mask based on all cytoplasmic stainings is automatically generated (the automatically generated measure mask is staining-dependent in its extension and adjustable to the appropriate cell size). The software then automatically measures the intensity for each channel and depicts co-localization of different fluorescent markers in form of scatter diagrams (FACS-like presentation).[20] The statistics including mean intensity are generated automatically after manual setting of cut-offs.

Statistical analysis

Statistical analysis was performed with Prism (Prism, version 4a, 2003; GraphPad Software, San Diego, CA, USA) and statistica (Statistica version 8, Statsoft Inc., Tulsa, OK, USA). Results are presented as mean ± SD. All normally distributed data sets (established from Kolmogorov–Smirnov tests) were compared using analysis of variance with Newman–Keuls *post hoc* test; non-normally distributed data sets were compared using Wilcoxon rank-sum test. Two-sided testing was used. Differences were considered significant at $P < 0.05$.

Results

Plasma and whole blood fluorescence

The plasma half-life of the fluorescent SPION was 328 ± 65 min in rats (*Figure 1*). The fluorescence measured on whole blood demonstrated a decrease in fluorescence over the first 18 h followed by an increase in fluorescence from Day 1 on (*Figure 1*). This kinetic corresponded to the disappearance of the fluorescent SPION from plasma and to the reappearance of fluorescent SPION inside cells (as measured in whole blood). The fluorescent SPION were associated with CD68-positive cells (monocytes/macrophages), but not with PMN. Hence, an i.v. injection of fluorescent SPION allowed loading the resting monocytes/macrophages *in vivo*. The liver and the spleen were also highly fluorescent (data not shown) and served as control for the i.v. injection of the fluorescent SPION.

Monocytes/macrophages tracking by magnetic resonance imaging

A delay of 3 days between i.v. injection of florescent SPION and ischaemia–reperfusion was used to allow for a complete disappearance of nanoparticles from the plasma. All animals in the SPION_MI group demonstrated a clear hypointense (black) signal in the MI area, whereas animals in the Ø_MI group never showed the hypointense signal (*Figure 2*). Magnetic resonance imaging acquired *ex vivo* correlated well with *in vivo* imaging, confirming the presence of a hypointense signal in the injected group and no hypointense signal in the non-injected group.

Ex vivo fluorescence showed accumulation of fluorescence with time into the MI in the SPION_MI group, but showed no fluorescence in the Ø_MI group (*Figure 2*).

Hence, *in vivo* and *ex vivo* imaging were capable of depicting gradual infiltration of pre-loaded monocytes/macrophages into the MI.

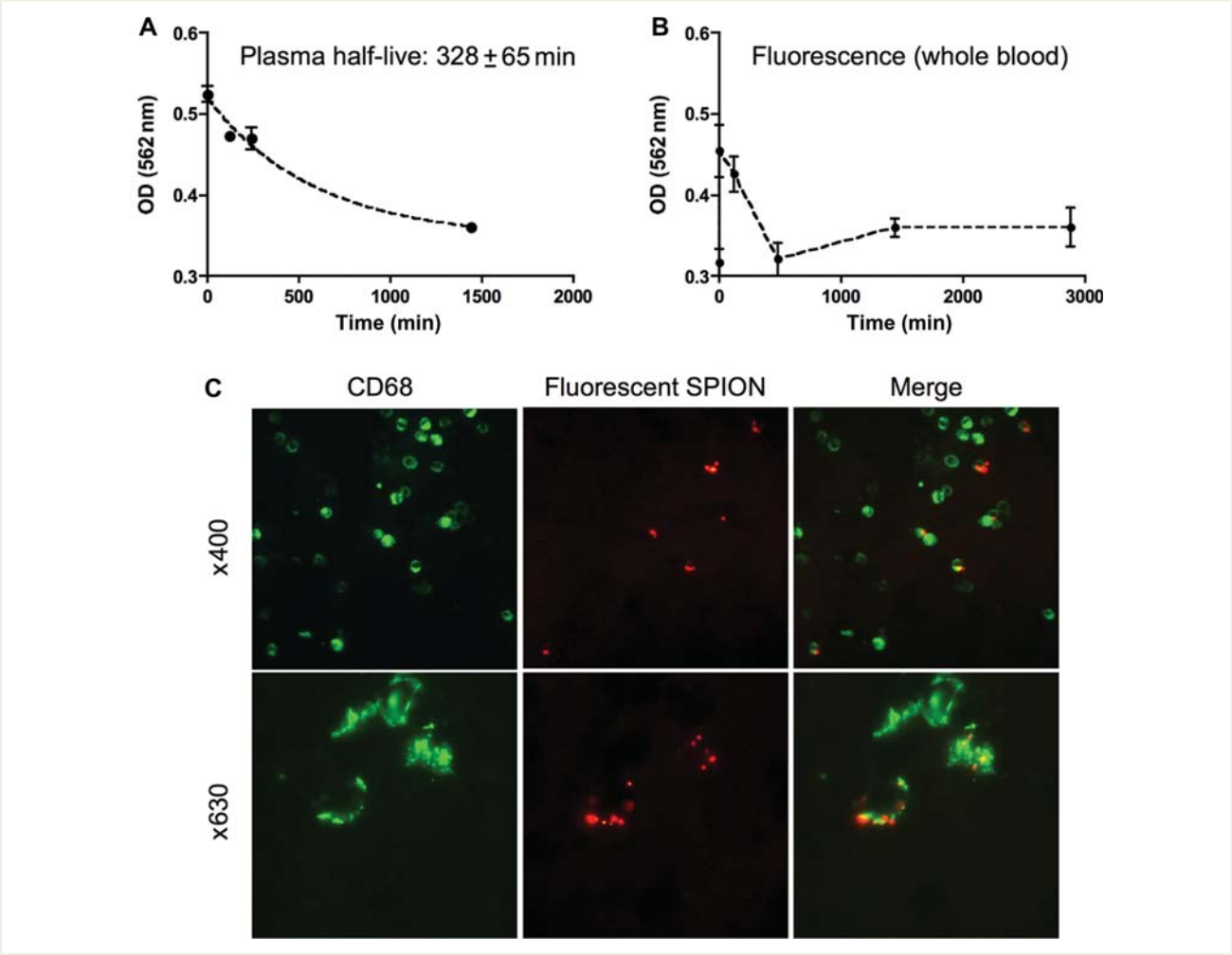

Figure 1 Plasma and whole blood fluorescence. Time course of fluorescent superparamagnetic iron oxide nanoparticles absorption in plasma (*A*) and whole blood (*B*). Plasma half-life was 328 ± 65 min. After an initial decrease in the fluorescence in whole blood, fluorescence reappeared (*B*) and is clearly associated with CD68-positive circulating cells (*C*). Hence, an intravenous injection of fluorescent superparamagnetic iron oxide nanoparticles allowed *in vivo* loading of monocytes.

Global cardiac function analysis

The global cardiac function was assessed through EF (*Table 1*). The EF of the SPION_Sham group was always higher than all other groups, reaching the statistical threshold only at Day 0. Nevertheless, one can see that the thoracotomy induces stress in the animal and that it takes 3 days for a normalization of the cardiac function. There were no statistical differences between the SPION_MI and the Ø_MI groups, indicating that the injection of iron *per se* has no impact on global cardiac function. The EF of the SPION_MI_AntiCCL5 group was higher than the SPION_MI group, without reaching the statistical level. As the primary goal of this paper was to image the inflammatory response following MI, we did not make any effort to optimize the antiCCL5 treatment. This will have to be done in future studies.

Regional cardiac function analysis

Regional cardiac function was assessed through MR tag analysis. The hypointense (black) signal appearing in the antero-lateral

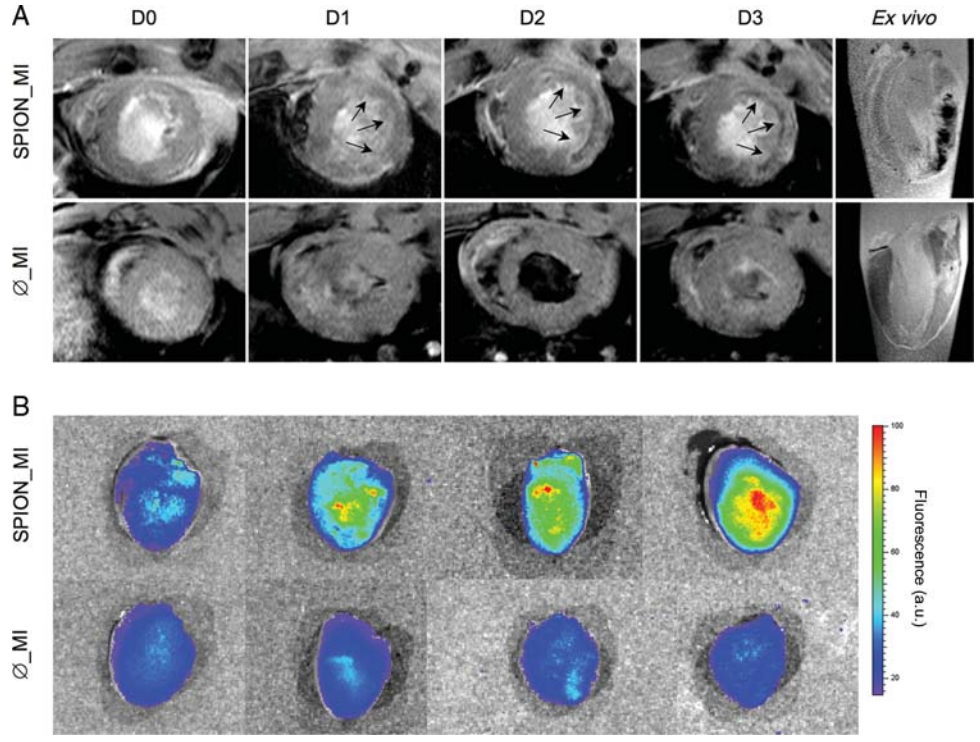

Figure 2 *In vivo* and *ex vivo* imaging. *In vivo* magnetic resonance imaging of the infarcted groups is presented in (*A*). The first line corresponds to a representative rat of the SPION_MI group and clearly shows the appearance over time [Day (D) 0 to D3] of a hypointense (black) signal in the myocardial infarction area (arrows). As discussed, the appearance of the hypointense signal is due to the superparamagnetic iron oxide. The second line corresponds to a representative rat of the Ø_MI group and does not show any hypointense signal. *Ex vivo* magnetic resonance imaging (last column) also depicts a clear hypointense signal in the SPION_MI rat, whereas no hypointense signal was seen in the Ø_MI, thus confirming the *in vivo* results. *Ex vivo* reflectance fluorescence (*B*) also confirmed the magnetic resonance results. A representative image of the injected group shows a clear increase in fluorescence over time, whereas the non-injected group does not show any fluorescent signal.

Table 1 Ejection fraction

	Ejection fraction (%)			
	D0	**D1**	**D2**	**D3**
SPION_Sham	76 ± 4 *	77 ± 3	79 ± 5	82 ± 5
SPION_MI	53 ± 11 *	62 ± 11	65 ± 12	67 ± 13
Ø_MI	58 ± 8	65 ± 8	70 ± 11	68 ± 13
SPION_MI_AntiCCL5	63 ± 9	70 ± 10	72 ± 6	72 ± 7

*$P < 0.05$.

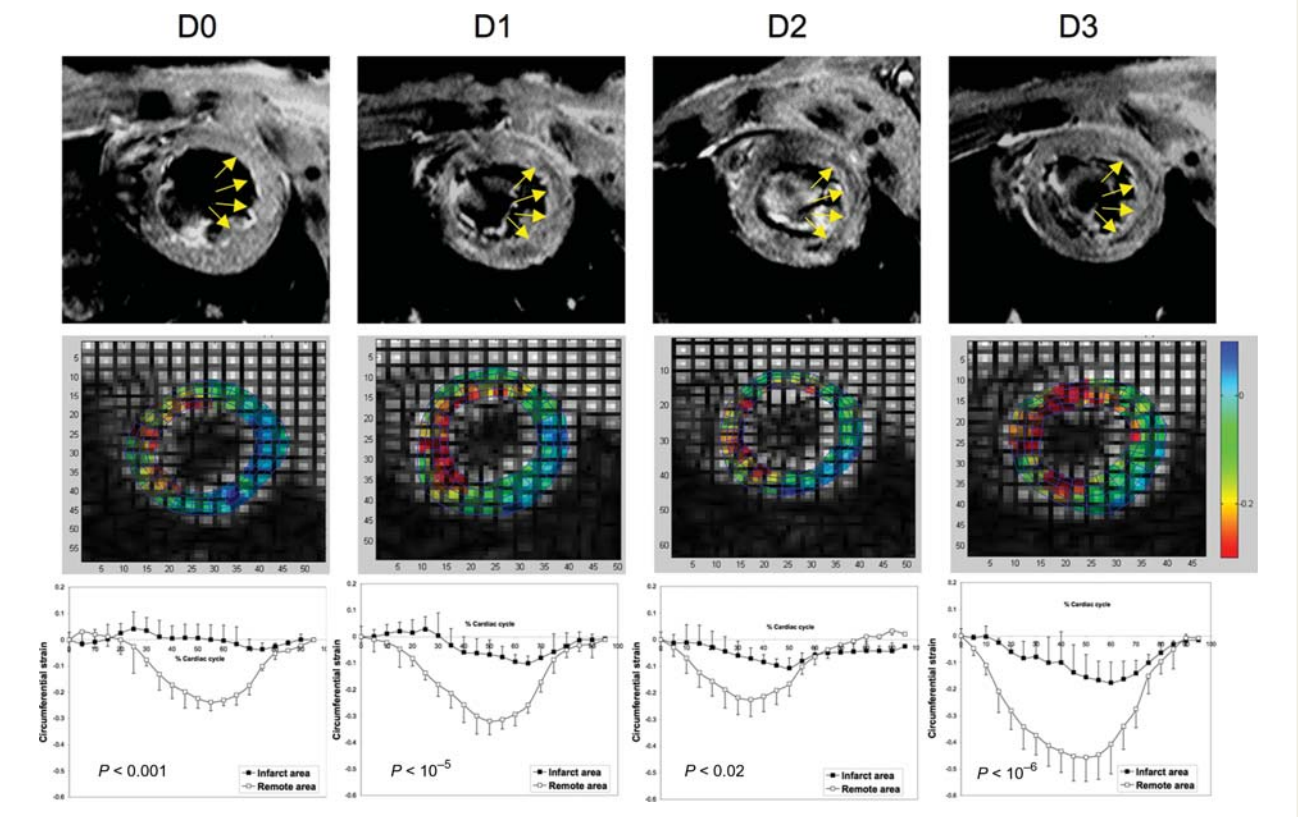

Figure 3 Regional cardiac function. Representative case of the SPION_MI groups. Magnetic resonance imaging are presented from Days 0 to 3 (first line), as well as colour-coded map of circumferential shortening (second line, akinesia been coded in blue and normal contraction being coded in red) and tag analysis (third line). This figure demonstrates that the hypointense (black) region corresponds to the hypokinetic part of the left ventricle and hence represents the arrival of iron in the myocardial infarction. Please note that the contraction of the hypointense region was always statistically different from the contraction of the remote region ($P < 0.02$, at least).

wall of the LV corresponded well with the hypokinetic part of the LV (*Figure 3*). Moreover, statistical analysis revealed a clear contraction difference ($P < 0.02$) between the normal and hypointense part of the LV (*Figure 3*).

Hence, the appearance of a hypointense signal corresponds to the appearance of iron, which in turn corresponds to the hypokinetic part of the LV and hence to MI.

Quantitation of the infiltration

Quantitation by histology

Immunohistochemistry against CD68-positive cells was used to quantify infiltration of the MI by monocytes/macrophages with time. Infiltration followed an exponential pattern from Days 0 to 3 (*Figure 4*). There were no differences in the number of monocytes/macrophages counted in the MI between the SPION_MI and the Ø_MI groups ($P > 0.5$) (*Figure 4A*). The number of monocytes/macrophages counted in the SPION_MI_antiCCL5 group was significantly lower than in the non-treated groups ($P < 0.001$) (*Figure 4A*). No monocytes/macrophages were seen in the myocardium of the SPION_Sham group.

Quantitation by magnetic resonance imaging

The acquisition of parametric T2 map allowed calculating T2 relaxation time. It is known that superparamagnetic iron oxide has a strong effect on T2 relaxation time. The more the iron, the shorter the T2 and the bigger the 1/T2.[21] The quantitation of iron content in the MI correlated well with the number of macrophages present in the MI in histology (*Figure 4C* and *Table 2*). Moreover, the intermediate number of monocytes/macrophages seen in the SPION_MI_AntiCCL5 group, corresponded to an intermediate 1/T2 value (*Figure 4* and *Table 2*). Nevertheless, further studies will be needed to directly compare the accuracy of MRI to quantify monocytes/macrophages infiltration with a classical gold standard such as immunohistology.

Different groups at Day 3

The SPION_MI group, showed clear infarcted area by MRI (akinesia of the antero-lateral wall) and by histology (fibrosis = 17.7 ± 3.4) at Day 3, as well as CD68-positive cells, containing iron (*Figure 5*). The Ø_MI group showed clear infarcted areas by MRI and by histology (fibrosis = 19.6 ± 8.2) containing numerous monocytes/macrophages, but iron oxide was never detected. The SPION_Sham group never showed signs of infarct, nor

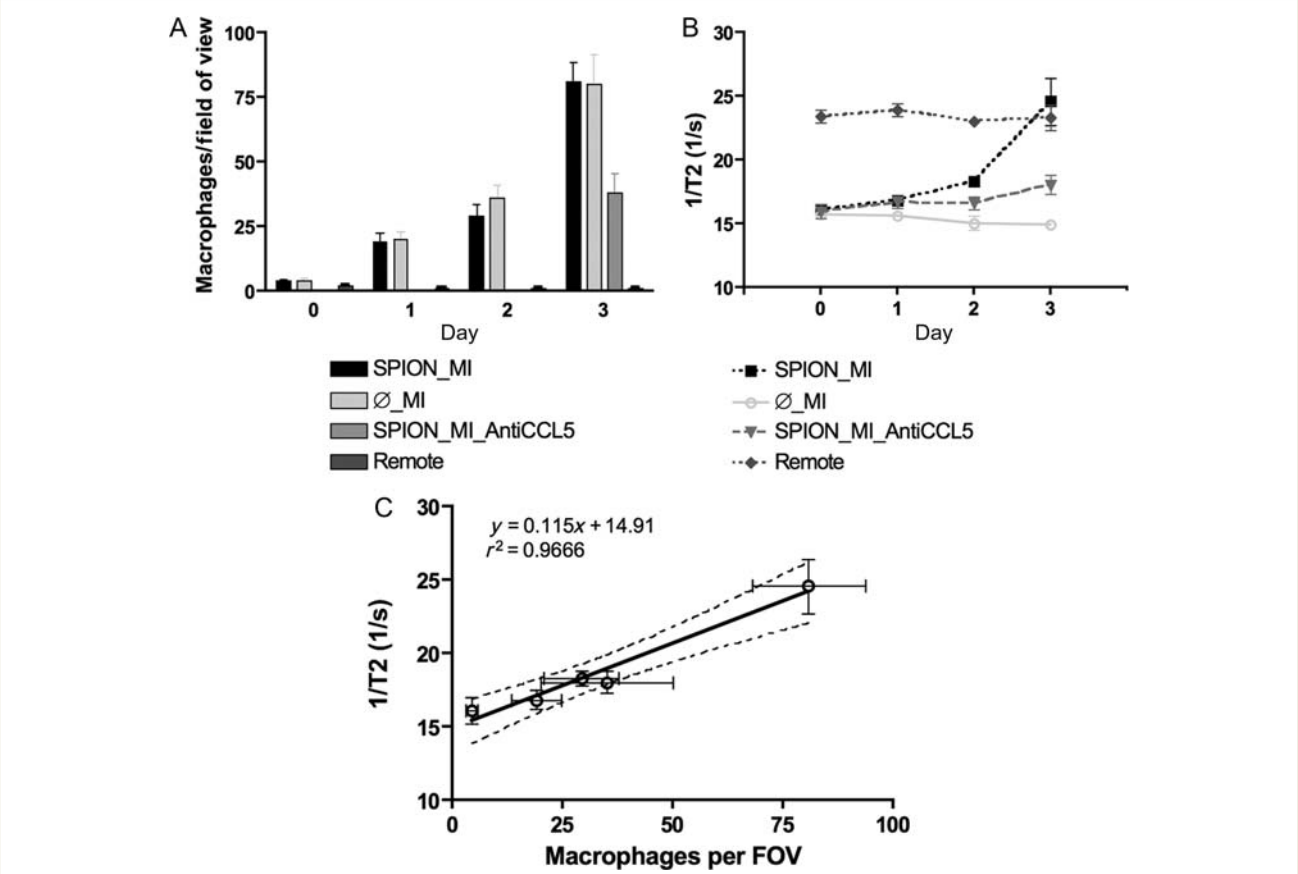

Figure 4 Monocytes/macrophages quantification. Monocytes/macrophages infiltration on histological myocardial slices is presented in (*A*). The infiltration showed an exponential growth over time. There was no difference in cellular infiltration between the SPION_MI and the Ø_MI groups, whereas the SPION_MI_AntiCCL5 showed a statistically lower monocytes/macrophages infiltration at Day 3 ($P < 0.001$). The quantitation of the 1/T2 values (*B*) correlated well with histological data (*C*). Hence, quantitation of the monocytes/macrophages infiltration of myocardial infarction *in vivo* by magnetic resonance imaging provides an excellent estimate of the number of macrophages, with an error <3%. Dashed line corresponds to 95% confidence interval.

monocytes/macrophages infiltration. The SPION_MI_AntiCCL5 group showed smaller infarcted area by MRI and by histology (fibrosis = 10.7 ± 5.5), with less numerous monocytes/macrophages infiltration than in the non-treated groups. The fibrosis of the SPION_MI-AntiCCL5 group was smaller than the fibrosis of both SPION_MI and Ø_MI ($P < 0.05$), and the number of CD68+ cells seen in SPION_MI_AntiCCL5 was also smaller than in the SPION_MI and Ø_MI groups ($P < 0.001$).

Automatic determination of loaded monocytes/macrophages on histological slices

Co-localization of CD68-positive cells with fluorescent SPION showed that the SPION_MI group had a mean loading of monocytes/macrophages of 81% (*Figure 6*). The Ø_MI group showed no loaded monocytes/macrophages. The SPION_Sham group showed no inflammatory cells infiltration. The SPION_MI_AntiCCL5 group showed a mean loading of monocytes/macrophages of 79%, which was not different from the SPION_MI group ($P > 0.5$), allowing to directly compare the T2 values (or 1/T2) between both groups. Having the same loading, so the same quantity of iron, changes in T2 (or 1/T2) reflects changes in cell numbers. Hence, the intermediate change of T2 (or 1/T2) in the SPION_MI_AntiCCL5 group corresponds to a lower monocytes/macrophages infiltration (when compared with the SPION_MI group).

Discussion

Iron oxide nanoparticles are cleared from the plasma by the RES. Part of the RES consists of resident macrophages of the liver (Kupffer cells). Even if these cells are clearly loaded with iron (data not shown), they will never be able to infiltrate inflammatory lesions, because they are incapable of leaving the liver (resident macrophages). Another part of the RES is formed by the monocytes. These cells are also loaded with fluorescent SPION (*Figure 1*) and, as they have the propensity to circulate, they are able to infiltrate inflammatory lesions.

All the papers previously published on iron oxide nanoparticles and imaging used an i.v. injection of the nanoparticles *after*

Table 2 T2 and 1/T2 values in the myocardial infarction and in the remote zone

	SPION-MI		
	Macrophages	T2 (ms)	1/T2 (s^{-1})
D0	4 ± 1	62 ± 6	16 ± 1.6
D1	19 ± 6	60 ± 4	16.8 ± 1.1
D2	29 ± 8	55 ± 3	18.3 ± 0.8
D3	79 ± 11	42 ± 6	24.6 ± 4.5
	Ø-MI		
	Macrophages	T2 (ms)	1/T2 (s^{-1})
D0	4 ± 2	64 ± 6	15.7 ± 1.5
D1	20 ± 5	64 ± 5	15.6 ± 1.1
D2	36 ± 9	67 ± 7	15.0 ± 1.5
D3	77 ± 15	67 ± 2	14.9 ± 0.5
	SPION-MI-AntiCCL5		
	Macrophages	T2 (ms)	1/T2 (s^{-1})
D0	NA	63 ± 5	15.9 ± 1.4
D1	NA	60 ± 4	16.7 ± 1.2
D2	NA	59 ± 3	16.6 ± 1.2
D3	35 +/- 15	55 ± 4	18.0 ± 1.8
	Remote		
	Macrophages	T2 (ms)	1/T2 (s^{-1})
D0	0 ± 1	43 ± 4	23.4 ± 2.0
D1	1 ± 1	42 ± 3	23.9 ± 1.6
D2	2 ± 1	43 ± 1	23.0 ± 0.7
D3	1 ± 2	44 ± 4	23.3 ± 2.4

All values were statistically different from the remote region except: SPION-MI was not different from all remote and SPION-MI-AntiCCL5-D3 was not different from remote-D2 and -D3.
*$P < 0.05$.
**$P < 0.001$.

induction of the pathological process, in already activated monocytes[22,23] or *ex vivo* cell loading.[6] As far as we know, no other studies report the use of iron oxide nanoparticles injection *before* the induction of an inflammatory lesion. This study was designed to first load the resting RES, to wait for the complete disappearance of the nanoparticles from the plasma, and then track the monocytes/macrophages cells up to an inflammatory lesion in the same animal.

The blood half-life of the fluorescent SPION we used was 328 min. By waiting 3 days between the i.v. injection and the creation of the inflammatory lesion, we can expect <0.025% of the injected dose to remain in plasma (3 days correspond to >12 plasma half-lifes). Hence, if iron appears in the inflammatory lesion, it could not originate from a simple extravasation from the blood.

Moreover, we have demonstrated that the i.v. injected fluorescent SPION reappeared in the circulating monocytes (and only monocytes) after 1–2 days. Hence, appearance of iron in the inflammatory lesion is due to monocytes/macrophages infiltration.

One major advantage of this approach, when compared with an injection of iron oxide nanoparticles after the beginning of the inflammatory process, is that appearance of iron in the lesion could only be due to infiltration of monocytes/macrophages. In the studies where the nanoparticles were injected after the beginning of the inflammatory process, the presence of iron could be due to two main mechanisms: (i) iron could extravasate and be endocytosed by macrophages already in the lesion and (ii) circulating monocytes could also be loaded during their blood residency time and then extravasate. Hence, this type of experiments does not allow to differentiate infiltration of newly loaded monocytes/macrophages from phagocytosis by resident macrophages of newly extravasated iron.

Cell tracking by MRI is a well-known technique.[6,24] For a specific cell (or a cluster of cells) to be distinguished from the complex anatomical background, the cell should contain a contrast medium visible by a given imaging modality. Such contrast medium for MRI includes gadolinium chelate, manganese, and iron oxide nanoparticles. We chose iron oxide nanoparticles for multiple reasons. First, as previously stated, iron oxide nanoparticles are cleared from the blood by the RES, allowing *in vivo* loading of the monocytes/macrophages. Secondly, the synthesis of fluorescent iron oxide nanoparticle was published,[25] allowing multimodal imaging and correlative histology. Thirdly, iron oxide nanoparticles are non-toxic for the cells and are not known to induce inflammation *per se*.[26] Hence, using fluorescent SPION allowed combining the advantage of *in vivo* imaging by MRI (using the iron as contrast medium) with the cellular localization obtained by fluorescence microscopy (using fluorophores as contrast media).

Ischaemia leading to infarction results in an inflammatory response. This response is accelerated and amplified in the case of reperfusion.[27] Mononuclear cells infiltration of the MI is governed sequentially by different proteins and chemokines. In the first few hours, C5a is wholly responsible for the mononuclear cells infiltration. After 60–180 min, transforming growth factor β1 (TGFβ1) contributes significantly to the chemotactic activity. After 180 min, MCP-1 acting together with TGFβ1 has a major role.[1,3,28] The majority (in terms of number) of inflammatory cells found in MI are macrophages, with a peak occurring between Days 3 and 4.[27,29] The presence of >1000 macrophages/mm^2 in the MI would facilitate their detection. As the maximal infiltration appeared around Days 3–4, animals were only sequentially studied for 4 days in this study (from Days 0 to 3).

In our model of ischaemia–reperfusion, a clear hypointense signal was detected over time in the MI, corresponding to infiltration of iron-loaded monocytes/macrophages. The presence of fluorescent SPION was detectable *in vivo*, *ex vivo* (by MRI and fluorescent imaging), and by histology. An anti-CCL5 treatment induced a lower monocytes/macrophages infiltration and a smaller infarct.

Despite the smaller MI, the anti-CCL5-treated groups did not show a better cardiac function than the untreated group. Nevertheless, as the primary goal of this study was to image the inflammatory process, we have not optimized the anti-inflammatory treatment. The animals received only one injection of the anti-inflammatory treatment during the reperfusion. Future studies aiming at determining the best anti-inflammatory treatment protocol has to be done, i.e. determine the dose and timing of anti-CCL5 injection for an optimal effect. Furthermore, the research group directed by Prof. Mach have recently tested the treatment with anti-RANTES agents in a mouse model of myocardial ischaemia–reperfusion. The results showed that a single i.p. injection of a

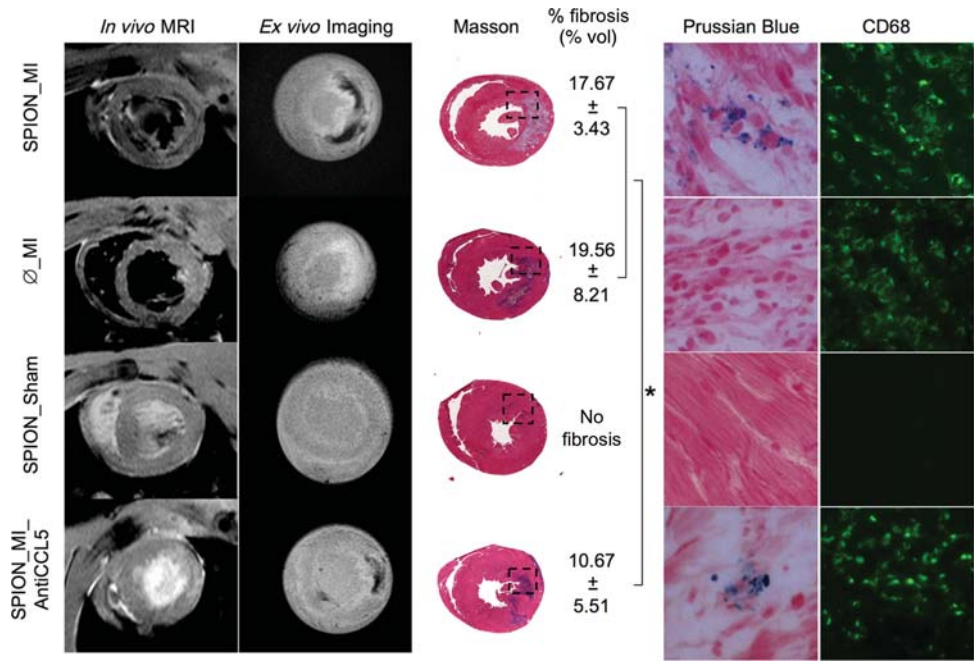

Figure 5 Comparison of all groups at Day 3. SPION_MI clearly showed a hypointense signal by magnetic resonance imaging (*in vivo* and *ex vivo*) in the myocardial infarction. The fibrosis of this group was calculated to 17.67 ± 3.43% (%vol). There were numerous fluorescent-loaded cells in the myocardial infarction, corresponding to CD68-positive cells. Ø_MI did not show hypointense signal by magnetic resonance imaging, or iron-loaded cells by histology. The fibrosis was 19.56 ± 8.21%. The SPION_Sham group did not show an inflammatory infiltrate or myocardial infarction. The SPION_MI_AntiCCL5 showed a hypointense signal by magnetic resonance imaging, smaller fibrosis (10.67 ± 5.51%) and less iron-loaded CD68-positive cells in the myocardial infarction. $*P < 0.05$.

RANTES Antagonist (AANA-RANTES) performed during ischaemia (5 min before the reperfusion) significantly reduces infarct size in wild type and apolipoproiten (Apo)$E^{-/-}$ mice (unpublished data). This effect may be related to the diminished leucocyte infiltration into the ischaemic myocardium during the reperfusion period (unpublished data).

Reperfusion inflammatory injury is considered an important factor in myocardial deterioration after acute coronary syndrome (ACS). Both local and systemic inflammatory reactions play a crucial role in this process. Indeed, the inhibition of leucocyte infiltration in the infarcted myocardial tissue represents a promising strategy to reduce reperfusion injury. In particular, the inhibition of pro-inflammatory molecules such as cytokines and chemokines, which orchestrate leucocyte trafficking, may be of potential benefit in post-ischaemic complications, including heart failure. RANTES has been shown to play a crucial role in the context of ACS.[30–32]

As many of the treatments used today in the context of MI also have potent anti-inflammatory effects, including angiotensin-converting enzyme inhibitors, beta-blockers, and statins,[2] imaging the inflammatory process during the treatment of MI should improve our understanding of the role of the monocytes/macrophages during healing. A recent paper[33] suggests that two different subtypes of monocytes/macrophages are responsible for the early inflammatory response and for the later 'reconstructive' process. Extracellular matrix degradation and removal of dead cardiomyocytes dominate in the early phase and weakened the heart wall. Angiogenesis and granulation tissue dominate in the late phase (after around 5 days) and promote healing. Hence, non-specific anti-inflammatory treatment should be applied with caution in the setting of MI. The visualization of monocytes/macrophages infiltration post-MI could help understanding the role of these cells in myocardial fate.

As inflammatory response is not only implicated in MI, but also in oncology[34] and rheumatoid arthritis,[35] we believe that this simple method of *in vivo* cell loading and *in vivo* cell tracking in the same animal would be helpful in other important models of the health problems of our society.

Expected clinical applications

As iron oxide nanoparticles have already been approved or are investigated in Phase III clinical studies, this paper may yield to numerous clinical applications. For instance, in the case of chronic coronary occlusion, revascularization is not performed in an emergency context but during a scheduled session. Therefore, monocytes loading using commercially available iron oxide nanoparticle could be performed before the revascularization procedure and the controversial effect of reperfusion on inflammatory response could then be studied non-invasively in patients. Nevertheless, this clinical application will have to be tested before, because revascularization of chronic coronary occlusion may not involved ischaemia–reperfusion damage as in the acute settings.

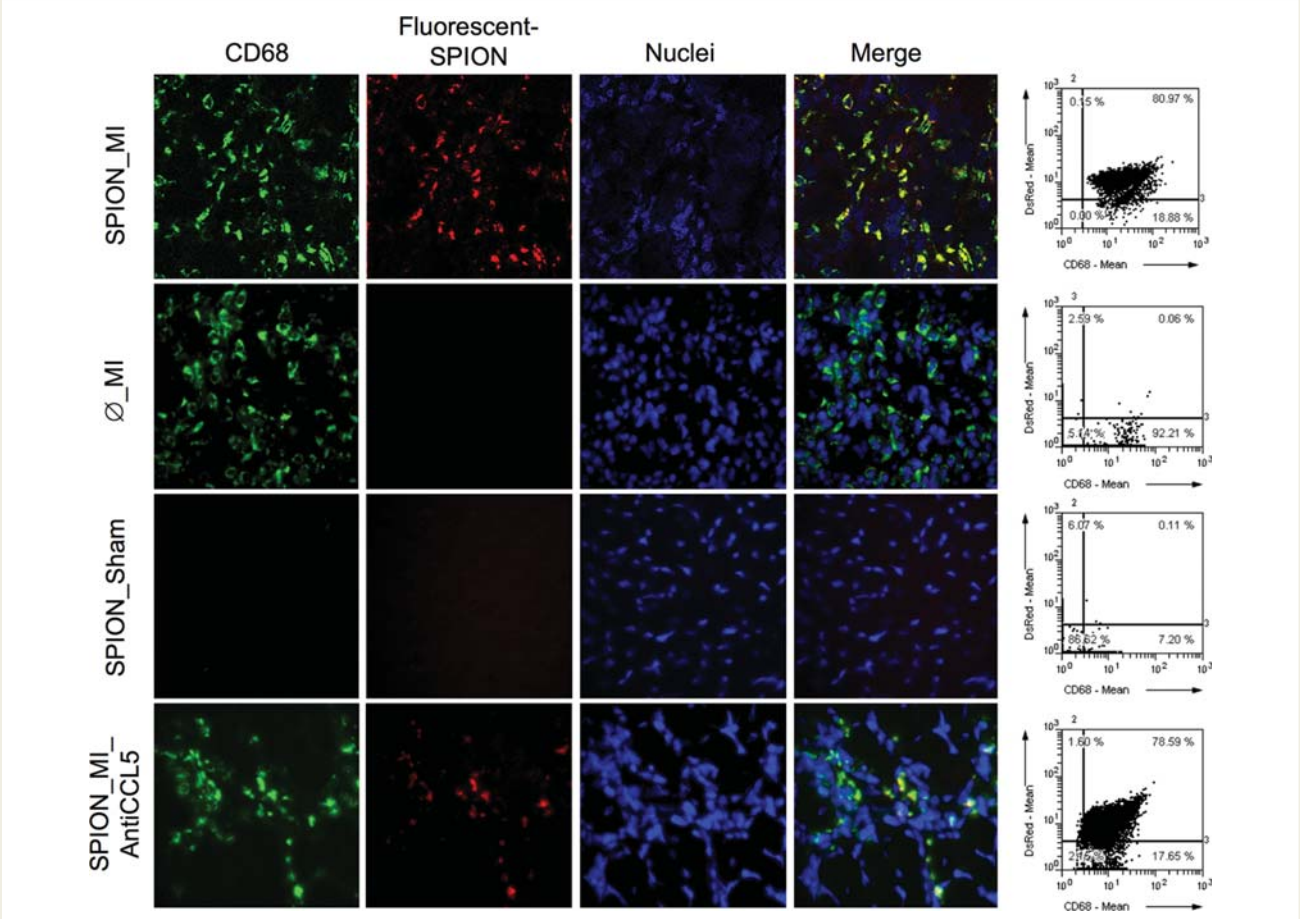

Figure 6 Cellular infiltration characterization. Cellular infiltration was characterized with TissueQuest®. The SPION_MI group showed that CD68-positive cells were loaded to 81%. The loading of monocytes/macrophages in the SPION_MI_AntiCCL5 group was also around 80%. Hence, even if the number of macrophages infiltrating the myocardial infarction was significantly lower in this group, the mean loading was in the same order.

Conclusion

This study demonstrates that resting monocytes/macrophages can be loaded *in vivo* by a simple i.v. injection of iron oxide nanoparticles and then tracked *in vivo* by MRI in the very same animal in a rodent model of MI. *Ex vivo* imaging (MRI and fluorescence) as well as histology correlated well with *in vivo* results, with the estimated number of macrophages *in vivo* by MRI showing $<3\%$ error compared with histological analysis. Furthermore, the good precision of the method allowed *in vivo* follow-up of the amount of inflammation-induced infiltrating monocytes/macrophages during an anti-CCL5 treatment.

Acknowledgements

The authors would like to thank Prof. Lee Josephson (Harvard Medical School) for helpful discussions and comments during the study.

Funding

This work was supported by the Swiss National Science Foundation (Grant number: 320030-116813 to X.M. and PP0033-116901 to J.-P.V.) and by the Boninchi foundation.

Conflict of interest: none declared.

References

1. Frangogiannis NG, Smith CW, Entman ML. The inflammatory response in myocardial infarction. *Cardiovasc Res* 2002;**53**:31–47.
2. Nian M, Lee P, Khaper N, Liu P. Inflammatory cytokines and postmyocardial infarction remodeling. *Circ Res* 2004;**94**:1543–1553.
3. Ren G, Dewald O, Frangogiannis NG. Inflammatory mechanisms in myocardial infarction. *Curr Drug Targets Inflamm Allergy* 2003;**2**:242–256.
4. Kakio T, Matsumori A, Ono K, Ito H, Matsushima K, Sasayama S. Roles and relationship of macrophages and monocyte chemotactic and activating factor/monocyte chemoattractant protein-1 in the ischemic and reperfused rat heart. *Lab Invest* 2000;**80**:1127–1136.
5. Kumar AG, Ballantyne CM, Michael LH, Kukielka GL, Youker KA, Lindsey ML, Hawkins HK, Birdsall HH, MacKay CR, LaRosa GJ, Rossen RD, Smith CW, Entman ML. Induction of monocyte chemoattractant protein-1 in the small veins of the ischemic and reperfused canine myocardium. *Circulation* 1997;**95**:693–700.
6. Rogers WJ, Meyer CH, Kramer CM. Technology insight: *in vivo* cell tracking by use of MRI. *Nat Clin Pract Cardiovasc Med* 2006;**3**:554–562.
7. Montet-Abou K, Montet X, Weissleder R, Josephson L. Cell internalization of magnetic nanoparticles using transfection agents. *Mol Imaging* 2007;**6**:1–9.
8. Kelley JL, Rozek MM, Suenram CA, Schwartz CJ. Activation of human blood monocytes by adherence to tissue culture plastic surfaces. *Exp Mol Pathol* 1987;**46**:266–278.
9. Bulte JW, Kraitchman DL. Iron oxide MR contrast agents for molecular and cellular imaging. *NMR Biomed* 2004;**17**:484–499.

10. Toso C, Vallee JP, Morel P, Ris F, Demuylder-Mischler S, Lepetit-Coiffe M, Marangon N, Saudek F, James Shapiro AM, Bosco D, Berney T. Clinical magnetic resonance imaging of pancreatic islet grafts after iron nanoparticle labeling. *Am J Transplant* 2008;**8**:701–706.
11. Chastellain M, Petri A, Hofmann H. Particle size investigations of a multistep synthesis of PVA coated superparamagnetic nanoparticles. *J Colloid Interface Sci* 2004; **278**:353–360.
12. Petri-Fink A, Hofmann H. Superparamagnetic iron oxide nanoparticles (SPIONs): from synthesis to *in vivo* studies—a summary of the synthesis, characterization, *in vitro*, and *in vivo* investigations of SPIONs with particular focus on surface and colloidal properties. *IEEE Trans Nanobioscience* 2007;**6**:289–297.
13. Braunersreuther V, Steffens S, Arnaud C, Pelli G, Burger F, Proudfoot A, Mach F. A novel RANTES antagonist prevents progression of established atherosclerotic lesions in mice. *Arterioscler Thromb Vasc Biol* 2008;**28**:1090–1096.
14. Montet-Abou K, Daire JL, Ivancevic MK, Hyacinthe JN, Nguyen D, Jorge-Costa M, Morel DR, Vallee JP. Optimization of cardiac cine in the rat on a clinical 1.5-T MR system. *Magma* 2006;**19**:144–151.
15. Daire JL, Jacob JP, Hyacinthe JN, Croisille P, Montet-Abou K, Richter S, Botsikas D, Lepetit-Coiffe M, Morel D, Vallee JP. Cine and tagged cardiovascular magnetic resonance imaging in normal rat at 1.5 T: a rest and stress study. *J Cardiovasc Magn Reson* 2008;**10**:48.
16. Ivancevic MK, Daire JL, Hyacinthe JN, Crelier G, Kozerke S, Montet-Abou K, Gunes-Tatar I, Morel DR, Vallee JP. High-resolution complementary spatial modulation of magnetization (CSPAMM) rat heart tagging on a 1.5 Tesla Clinical Magnetic Resonance System: a preliminary feasibility study. *Invest Radiol* 2007;**42**: 204–210.
17. Messroghli DR, Bainbridge GJ, Alfakih K, Jones TR, Plein S, Ridgway JP, Sivananthan MU. Assessment of regional left ventricular function: accuracy and reproducibility of positioning standard short-axis sections in cardiac MR imaging. *Radiology* 2005;**235**:229–236.
18. Rehr RB, Malloy CR, Filipchuk NG, Peshock RM. Left ventricular volumes measured by MR imaging. *Radiology* 1985;**156**:717–719.
19. Jacob J, Vachier C, Morel J, Daire JL, Hyacinthe JN, Vallee JP. Extrema Temporal Chaining: a new method for computing the 2D Displacement Field of the Heart from Tagged MRI. *Lect Notes Comput Sci* 2006;**4179**:897–908.
20. Streit M, Ecker RC, Osterreicher K, Steiner GE, Bischof H, Bangert C, Kopp T, Rogojanu R. 3D parallel coordinate systems—a new data visualization method in the context of microscopy-based multicolor tissue cytometry. *Cytometry A* 2006;**69**:601–611.
21. Riviere C, Boudghene FP, Gazeau F, Roger J, Pons JN, Laissy JP, Allaire E, Michel JB, Letourneur D, Deux JF. Iron oxide nanoparticle-labeled rat smooth muscle cells: cardiac MR imaging for cell graft monitoring and quantitation. *Radiology* 2005;**235**: 959–967.
22. Jaffer FA, Nahrendorf M, Sosnovik D, Kelly KA, Aikawa E, Weissleder R. Cellular imaging of inflammation in atherosclerosis using magnetofluorescent nanomaterials. *Mol Imaging* 2006;**5**:85–92.
23. Sosnovik DE, Nahrendorf M, Deliolanis N, Novikov M, Aikawa E, Josephson L, Rosenzweig A, Weissleder R, Ntziachristos V. Fluorescence tomography and magnetic resonance imaging of myocardial macrophage infiltration in infarcted myocardium *in vivo*. *Circulation* 2007;**115**:1384–1391.
24. Gimi B, Artemov D, Leong T, Gracias DH, Gilson W, Stuber M, Bhujwalla ZM. Cell viability and noninvasive *in vivo* MRI tracking of 3D cell encapsulating self-assembled microcontainers. *Cell Transplant* 2007;**16**:403–408.
25. Funovics M, Montet X, Reynolds F, Weissleder R, Josephson L. Nanoparticles for the optical imaging of tumor E-selectin. *Neoplasia* 2005;**7**:904–911.
26. Oude Engberink RD, van der Pol SM, Dopp EA, de Vries HE, Blezer EL. Comparison of SPIO and USPIO for *in vitro* labeling of human monocytes: MR detection and cell function. *Radiology* 2007;**243**:467–474.
27. Vandervelde S, van Amerongen MJ, Tio RA, Petersen AH, van Luyn MJ, Harmsen MC. Increased inflammatory response and neovascularization in reperfused vs. non-reperfused murine myocardial infarction. *Cardiovasc Pathol* 2006;**15**: 83–90.
28. Frangogiannis NG. Chemokines in the ischemic myocardium: from inflammation to fibrosis. *Inflamm Res* 2004;**53**:585–595.
29. Fishbein MC, Maclean D, Maroko PR. Experimental myocardial infarction in the rat: qualitative and quantitative changes during pathologic evolution. *Am J Pathol* 1978;**90**:57–70.
30. Matsumoto N, Nomura S, Kamihata H, Kimura Y, Iwasaka T. Association of platelet-derived microparticles with C-C chemokines on vascular complication in patients with acute myocardial infarction. *Clin Appl Thromb Hemost* 2002;**8**: 279–286.
31. Parissis J, Filippatos G, Nikolaou V, Adamopoulos S. Cytokines and anti-cytokine therapeutic approaches to chronic heart failure. *Eur J Intern Med* 2002;**13**:356.
32. Steppich BA, Moog P, Matissek C, Wisniowski N, Kuhle J, Joghetaei N, Neumann FJ, Schomig A, Ott I. Cytokine profiles and T cell function in acute coronary syndromes. *Atherosclerosis* 2007;**190**:443–451.
33. Nahrendorf M, Swirski FK, Aikawa E, Stangenberg L, Wurdinger T, Figueiredo JL, Libby P, Weissleder R, Pittet MJ. The healing myocardium sequentially mobilizes two monocyte subsets with divergent and complementary functions. *J Exp Med* 2007;**204**:3037–3047.
34. Borrello MG, Degl'innocenti D, Pierotti MA. Inflammation and cancer: the oncogene-driven connection. *Cancer Lett* 2008;**267**:262–270.
35. Simmonds RE, Foxwell BM. Signalling, inflammation and arthritis: NF-kappaB and its relevance to arthritis and inflammation. *Rheumatology (Oxford)* 2008;**47**: 584–590.